Astron. Astrophys. 339, 811–821 (1998)

ASTRONOMY AND ASTROPHYSICS

Molecular line observations of southern S stars

J.H. Bieging[1], **L.B.G. Knee**[2], **W.B. Latter**[3], **and H. Olofsson**[4]

[1] Steward Observatory, The University of Arizona, Tucson, AZ 85721, USA
[2] National Research Council of Canada, Herzberg Institute of Astrophysics, Dominion Radio Astrophysical Observatory, P.O. Box 248, Penticton, BC V2A 6K3, Canada
[3] Infrared Processing and Analysis Center, Caltech, MS 100-22, Pasadena, CA 91125, USA
[4] Stockholm Observatory, S-133 36 Saltsjöbaden, Sweden

Received 26 March 1998 / Accepted 24 August 1998

Abstract. We observed a sample of southern S stars with the SEST telescope, in the SiO (v=0, J=3-2) transition at 130.3 GHz, and the HCN (J=1-0) transition at 88.6 GHz. SiO emission was detected in all seven stars observed, while HCN was detected in two. We employed a statistical equilibrium/radiative transfer model to estimate the SiO abundance for an assumed molecular distribution. The inferred SiO abundances are consistent with formation of the molecule under thermodynamic equilibrium (TE) conditions near the stellar photosphere, for reasonable physical conditions. We also model the HCN emission by a similar analysis, and find that if HCN is produced near the stellar photosphere, our model abundances are much higher than predicted by TE chemistry, unless the gas temperature is $<$1300 K and the gas density n(H_2) $\sim 10^{12}$ cm^{-3}. Under such conditions, condensation of silicate grains may enhance production of HCN for C/O ≈ 1. Alternatively, HCN may be formed by photochemical reactions in the outer circumstellar envelope, as has been proposed for O-rich giants.

Key words: stars: chemically peculiar – circumstellar matter – stars: mass-loss – stars: AGB

1. Introduction

S stars are a relatively rare class of red giants with optical spectra showing ZrO bands, a principal criterion defining the S spectral class. Analyses of their spectra reveal a photospheric C/O abundance ratio which is close to 1 (within 5%), and evidence of strong enrichment in s-process elements. In the past few years it has become clear that some S stars show technetium, while others do not. Jorrissen & Mayor (1992) and Van Eck et al. (1998) have shown that S stars without technetium are probably low-mass stars on the red giant or early asymptotic giant branch (AGB), whose surface abundances were altered by mass transfer from a binary companion. These stars are referred to as "extrinsic" S stars. In contrast, those S stars with technetium have luminosities placing them on the thermally pulsing (TP) AGB, with surface abundances altered by convective dredge-up (Van Eck et al. 1998). These objects are referred to as "intrinsic" S stars. The identification of technetium, which has no stable isotope, is a clear indicator of recent mixing of s-process elements to the surface. It has been suggested that S stars may be transition objects on the AGB, between the M-giants with C/O < 1, and the carbon stars (C/O > 1). Their relative rarity may imply a short timescale during which the photospheric C/O ratio passes from O-rich to C-rich, but this hypothesis is controversial (Zuckerman & Maddalena 1989; de Jong 1989; Chan & Kwok 1991).

A molecular line survey of 27 S stars by Bieging & Latter (1994, hereafter BL) detected CO J=1-0 or 2-1 emission from 13 stars, for which mass loss rates were derived. For the stars showing CO emission, BL also detected emission from HCN in 4 objects and from SiO in 8. The relatively high detection rates, and chemical model calculations for the photospheric abundances of HCN, SiO, and other chemical species, suggested that the chemical composition of the circumstellar envelope (CSE) is very sensitive to the C/O ratio at or near the stellar photosphere. In the simplest interpretation, the presence of SiO should be indicative of an O-rich composition, while HCN should point to a C-rich photosphere. Molecular line surveys of M- and C-stars by Bujarrabal et al. (1994), and Olofsson et al. (1993, 1998), as well as the S star study by BL, showed that both HCN and SiO are detectable in all categories of AGB stars. The observed ratio of emission line intensities for HCN (J=1-0) and SiO (J=2-1) are well-correlated with the C/O ratio of the stellar photosphere, as shown by Olofsson et al. (1998). In this respect, the HCN/SiO intensity ratios for S stars detected by BL are, in the mean, precisely between the mean ratios for M-type and C-type AGB stars, which is consistent with their values of C/O near unity, i.e., intermediate between M and C stars.

The molecular line survey of BL suggested that S stars have, on average, a dust/gas ratio in their CSEs which is a factor of 2 lower than for carbon stars. This result depends on the dust model used to derive dust masses from IR fluxes, though a separate study by Sahai & Liechti (1995) reached a similar conclusion, i.e., that the dust/gas ratio in S stars is lower than in other AGB stars. In this connection, it is significant that the S stars which have been observed with mid-IR interferometry show

Send offprint requests to: J. Bieging, (jbieging@as.arizona.edu)

Table 1. Source list and stellar properties

Star	IRAS	S2 no.[a]	K	IRAS fluxes		Spectral	Var.	Distance	$V_{\rm LSR}$	$V_{\rm e}$
			(mag)	S_{12} (Jy)	S_{60} (Jy)	Type	Type	(pc)	(km/s)	(km/s)
R Gem	07043+2246	307	2.12	21.6	2.34	S5/5	Mira	1100	-59.1	5.4
ST Sco	16334–3107	931	0.54	51.8	4.49	S8/4var	SRa	540	-4.5	7.1
RT Sco	17001–3651	954	0.34	161.	18.8	S7,2	Mira	490	-44.5	11.0
W Aql	19126–0708	1115	0.84	1575.	112.	S6/6e	Mira	610	-24.0	18.7
DK Vul	20044+2417	1189	1.70	18.6	3.8	S4,2	SRa	910	-14.2	5.0
RZ Sgr	20120–4433	1196	1.30	38.2	10.1	S4,4	SRb	760	-31.2	8.8
π^1 Gru	22196–4612	1294	-2.14	909.	77.	S5,7:	SRb	155	-12.5	11.0

[a] *A General Catalog of S Stars, 2nd Edition* (Stephenson 1984)

dust shells with inner radii which are significantly larger than is typical of M-type Miras or carbon stars (Danchi & Bester 1995). The S stars χ Cyg and W Aql have strong emission from both SiO and HCN (see BL), which is inconsistent with standard chemical models for formation under equilibrium conditions. Sharp (1988–see also Sharp & Wasserburg 1995), in theoretical chemical models which include grain condensation, finds that HCN formation can be strongly enhanced in even a slightly O-rich stellar atmosphere, if the oxygen in the gas phase is sufficiently depleted by condensation of silicate grains. Alternatively, HCN may be a product of photochemical reactions in the outer envelope. In O-rich stars showing detectable HCN emission, previous studies have argued that HCN is produced by a circumstellar photochemistry (e.g., Nercessian et al. 1989, Willacy & Millar 1997), but this interpretation is not without difficulties (Olofsson et al. 1998).

Since S stars as a class seem to be characterized by a C/O ratio near unity, they are of particular interest in examining the interplay of elemental abundances, dust formation, and envelope chemical composition in mass-losing AGB stars. For that reason, we were motivated to extend the molecular line survey of BL to a sample of S stars in the southern hemisphere. In this paper, we report the results of observations made with the Swedish-ESO Submillimetre Telescope (SEST)[1] of a sample of southern S stars for emission from both HCN and SiO. From the observed line intensities, we attempt to constrain the molecular abundances using statistical equilibrium models for a reasonable combination of model parameters. Finally, we compare our results with those obtained by others for mass-losing M- and C-stars on the AGB.

2. Observational results

2.1. Source selection

The sample consists of stars in *A General Catalog of S Stars, 2nd Edition* (Stephenson 1984, hereafter S2), for which CO J=1-0 or J=2-1 emission was well-detected by Sahai & Liechti (1995) or BL, and with nominal distances $\lesssim$ 1 kpc. Table 1 lists the seven S stars included in the sample. The first 3 columns give the variable star name; the IRAS Point Source Catalog (PSC) designation; and the S2 catalog number. Column 4 gives the K-band (λ2.2 μm) magnitude from the *Two Micron Sky Survey* (TMSS—Neugebauer & Leighton 1969) or from Gezari et al. (1993) if not in the TMSS. The 12 μm and 60 μm flux densities from the IRAS PSC are listed in columns 5 and 6. The spectral type in column 7 is taken from S2. (Note that S2 uses more than one variant of the S classification system, as indicated by the different formats in Table 1.) The variable star type is listed in column 8.

The estimated distance is given in column 9 of Table 1, and follows Jura (1988) and BL in assuming that all S stars have the same mean absolute K magnitude, $M_{\rm K}$ = -8.1 mag. For π^1 Gru, the *Hipparcos* parallax yields a distance of 153 pc (van Eck et al. 1998), essentially identical to that in Table 1, which was derived from the observed K magnitude and the assumed $M_{\rm K}$ of -8.1 mag. A typical variation in K-band luminosity of a factor of 2 between maximum and minimum light (cf. Jorissen & Knapp 1998) would cause a distance uncertainty of up to 40%. The assumed mean $M_{\rm K}$ is another potential error source. Groenewegen & deJong (1998) have used *Hipparcos* data to derive a mean $M_{\rm K}$ of -7.1 mag for semiregular and irregular variables among the intrinsic S stars. An error of 1 mag in our assumed $M_{\rm K}$ would result in a 60% overestimate in the distance in Table 1. A comparison of the distances in Table 1 with those of Groenewegen & deJong (1998) shows that the Miras agree to within 10%, while the 3 SRs without a measured parallax differ by the expected factor 1.6. π^1 Gru, however, is an SRb variable, yet has $M_{\rm K}$ = -8.0 (based on the *Hipparcos* distance), in good agreement with our adopted value of -8.1.

Finally, column 10 of Table 1 gives the systemic velocity (in the Local Standard of Rest) as determined from the CO 1-0 or 2-1 spectra obtained by BL or by Sahai & Liechti (1995). Column 11 lists our adopted envelope expansion velocity, $V_{\rm e}$, which we take as the average value derived from all published CO spectra, given by Jorissen & Knapp (1998).

All the stars in our sample show IR excesses in their IRAS fluxes, and all have relatively strong CO emission lines. Both

[1] The Swedish-ESO Submillimetre Telescope (SEST) is operated jointly by ESO and the Swedish National Facility for Radio Astronomy, Onsala Space Observatory at Chalmers University of Technology.

characteristics imply that these stars possess dusty circumstellar envelopes produced by mass loss, and so are probably intrinsic S stars on the TP-AGB. The presence of technetium has been verified spectroscopically in R Gem (Little et al. 1987) and π^1 Gru (Jorissen et al. 1993), thereby confirming that these two objects are intrinsic S stars. The IR colors of the other stars in the sample provide strong evidence that they are also intrinsic S stars, even though spectroscopic data for Tc are lacking. Specifically, Jorissen & Knapp (1998) find that all the stars in our sample lie in regions of the (K-[12], [25]-[60]) IR color-color diagram which are populated by *bona fide* intrinsic S stars, for which Tc is identified spectroscopically. We conclude, therefore, that our sample consists exclusively of intrinsic S stars.

2.2. Observations and data reduction

The millimetre wavelength spectroscopic observations were made using the 15 metre Swedish-ESO Submillimetre Telescope (Booth et al. 1989) in October and December 1995. The SESIS closed-cycle cryogenic receiver was used in dual frequency mode, enabling simultaneous observations of the HCN(J=1-0) lines near 88.6 GHz (three hyperfine components) and the SiO(v=0, J=3-2) line at 130.3 GHz. The spectra were integrated in two wide band acousto-optic spectrometers (Schieder et al. 1989) having a spectral resolution of 1.4 MHz (4.7 km s^{-1} at HCN, 3.2 km s^{-1} at SiO). Typical single sideband system temperatures were 140 K at HCN and 180 K at SiO.

Observations were made using a symmetric dual beam switching technique (focal plane chopping at 6 Hz, telescope nodding once every 2 minutes of time, chopping/nodding throw ~ 12 arc minutes in azimuth) which provided excellent compensation for short term atmospheric fluctuations and resulted in consistently flat baselines. The observations were initially calibrated to the T_A^* temperature scale (Kutner & Ulich 1981; Kutner et al. 1984) using the cooled chopper wheel technique. The absolute pointing accuracy of the telescope was 4 arc seconds rms, and was monitored by making occasional observations of IRC+10°216 and χ Cygni.

The data reduction followed standard procedures. Individual spectra were baselined (linear) and co-added with weights based upon the rms noise. The final spectra in T_A^* were converted to main beam brightness temperatures using main beam efficiencies η_{mb} of 0.75 (HCN) and 0.69 (SiO). The FWHM beam size is $56''$ for the HCN lines and $40''$ for the SiO line.

2.3. Results

Table 2 summarizes the observational results for the program S stars, as well as for the carbon star IRC+10^{o}216, which was observed to check the telescope calibration by comparison with results from other telescopes. The integration time includes both source and reference beam measurements. Columns 3 – 7 give the following quantities for the SiO (v=0, J=3–2) transition : (a) peak main-beam brightness temperature; (b) line center velocity; (c) line full-width at half-maximum intensity; (d) rms noise level (mK-main beam brightness temperature) for off-line spectrometer channels; (e) intensity integrated over the line, in units of main-beam brightness temperature times velocity. Quantities (a), (b), and (c) were determined by a fit of the data to a gaussian line profile, using the least-squares fitting routine GAUSS in the *CLASS* software package of the Grenoble Astrophysics Group. Observations of M giants –e.g., Bujarrabal et al. 1989–show that SiO lines from these stars are typically gaussian-like, rather than parabolic or flat-topped profiles as are commonly found in CO emission from red giant envelopes. Within the noise, the gaussian fits give good representations of the observed SiO (v=0, J=3–2) line profiles.

Spectra of the SiO (v=0, J=3–2) detections for all the S stars and for IRC+10^{o}216 are shown in Fig. 1. For DK Vul and R Gem, the lines are weak relative to the noise level but show emission at velocities consistent with the well-detected CO emission lines, so we believe these stars are detected, though the derived line parameters are not well-determined (indicated by a colon in Table 2). The other 5 stars show clear detections at the velocities expected from the CO lines. The gaussian fits with parameters in Table 2 are shown as thin lines in Fig. 1.

Parameters for the HCN (1-0) line are given in columns 8 - 12 of Table 2. In this case, we have fitted parabolic profiles with the "SHELL" option of the *CLASS* software. Column 8 gives the peak intensity of the fit. Columns 9 and 10 show the center velocity and (FWZI)/2 of the fit. The rms noise of the off-line channels is in column 11, and the integrated intensity of the line (over the FWZI) is in the last column. We note that the HCN (1-0) line is significantly broadened by the presence of hyperfine structure, as is obvious in the spectrum of IRC+10°216, though the line shape is basically parabolic. For W Aql and IRC+10°216, hfs produces a (FWZI)/2 which is larger than the expansion velocity, V_e, while for RT Sco the width of the fit is affected by the low signal to noise ratio of the spectrum. For the detected S stars, the HCN spectra are too noisy to justify a deconvolution of the hfs components, so we have used only a single-component parabolic fit.

For non-detections of HCN, the upper limit to the integrated intensity, $I_{\rm mb}$, is taken to be an assumed linewidth given by the FWZI of the CO line from Sahai & Liechti (1995) or BL, multiplied by a peak-to-peak value of the noise, of 4 $\times$ RMS. These assumptions should give a conservative upper limit to $I_{\rm mb}$.

Spectra of the HCN J=1-0 line for the 2 detected S stars as well as IRC+10^{o}216 are shown in Fig. 2. The thin curves show the parabolic fits to the spectra. The HCN line was detected previously in W Aql by BL, who reported an integrated line intensity, $I_{\rm mb}$, of 2.75 K km s^{-1}, obtained with the NRAO 12-metre telescope. This value, when scaled by the ratio of the SEST and NRAO telescope areas, gives a predicted SEST intensity of 4.3 K km s^{-1}, provided the source is unresolved in both telescope beams. Our measured value (see Table 2) of 4.5 K km s^{-1} agrees to better than 5% with the predicted value, which indicates that the calibrations of the 2 telescopes are consistent. (At the distance of W Aql–610 pc–the HCN emission is almost certainly unresolved in the $56''$ SEST beam.) For comparison,

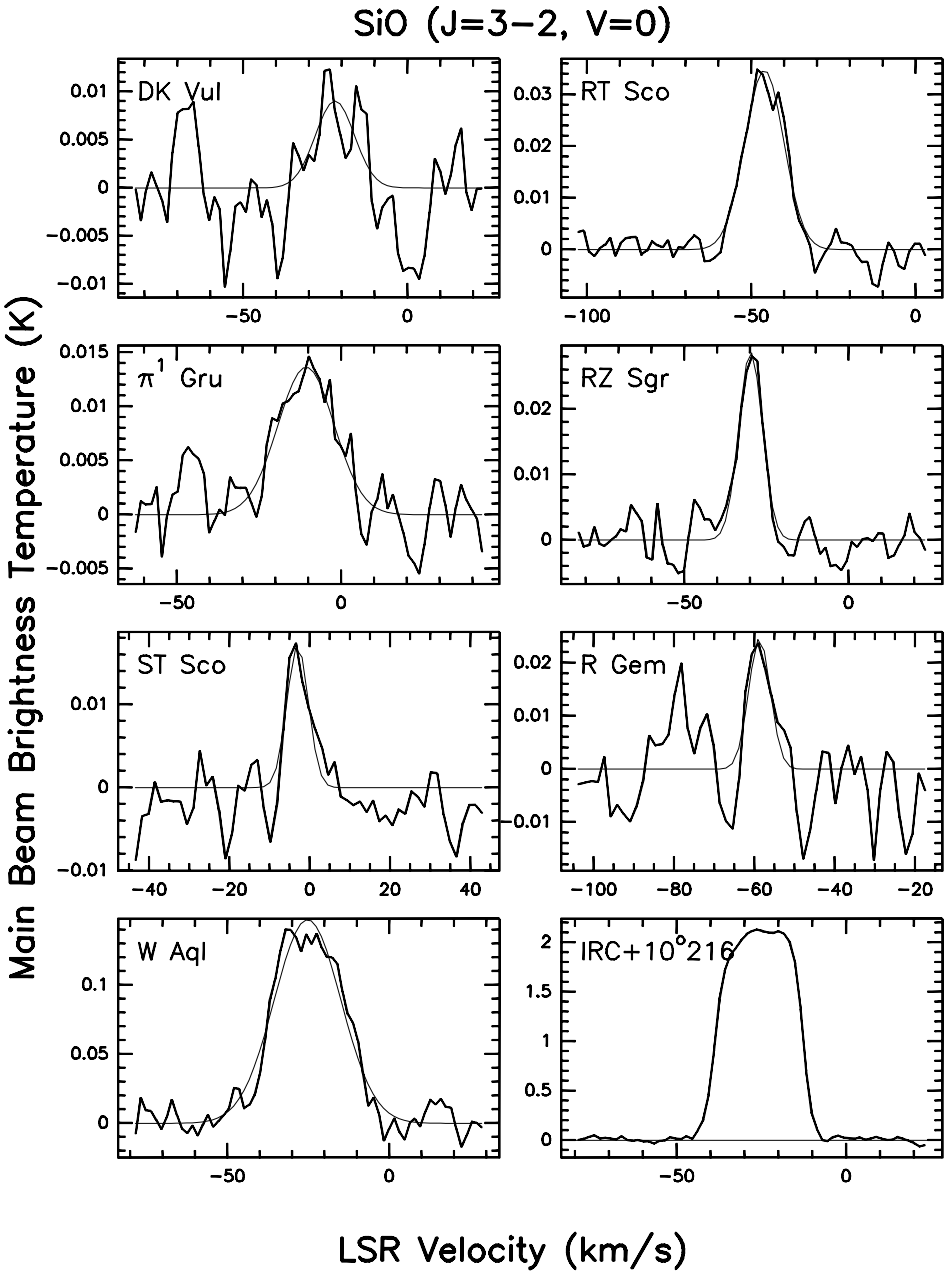

Fig. 1. Spectra of SiO (v=0, J=3-2) lines for all detected S stars and for the carbon star IRC+10^{o}216. For the S stars, the thin line shows the gaussian least-squares fit with parameters given in Table 2.

the carbon star IRC+10°216 has an integrated HCN intensity from Table 2 of 199 K km s^{-1}, while the scaled intensity from BL is 176 K km s^{-1}. The discrepancy may be attributed to the large angular size of the HCN emission from IRC+10°216 (Dayal & Bieging 1995), which is significantly resolved by the SEST beam.

3. Molecular abundance estimates

The determination of molecular abundances from the observed emission lines is ambiguous, mainly because the spatial distribution of the SiO and HCN emission is not known for these stars. Even so, we can make reasonable assumptions about the physical properties of the circumstellar envelopes (CSEs) to place constraints on the range of molecular abundances consistent with our observed line intensities. The range of derived SiO abundances for our program stars typically spans about one order of magnitude because of the sensitivity to the assumed physical size of the SiO distribution. The chemical equilibrium abundances of species like SiO and HCN, however, are very sensitive to temperature, density, and C/O ratio, spanning many orders of magnitude for reasonable "photospheric" parameter values, as shown in BL. Thus, despite the substantial dependence of the derived abundances on the assumed molecular distribution, it is possible to place some constraints on the physical conditions in the extended stellar atmophere where the SiO forms. For HCN, the formation mechanism is not known with any certainty, and only 2 stars in our sample are detected, so the usefulness of abundance constraints is perhaps more limited.

Table 2. Summary of observations

Star	Int. Time (min)	SiO (v=0,J=3-2) $T_{\rm mb}^a$ (K)	$V_{\rm o}^a$ (km/s)	FWHM^a (km/s)	RMS (mK)	$I_{\rm mb}$ (K km/s)	HCN (J=1-0) $T_{\rm mb}^b$ (K)	$V_{\rm o}^b$ (km/s)	FWZI/2^b (km/s)	RMS (mK)	$I_{\rm mb}$ (K km/s)
R Gem	52	0.025:	-58.6:	6.4:	6.8	0.13	—	—	—	6.7	<0.26
ST Sco	112	0.017	-2.9	6.3	4.2	0.10	—	—	—	4.1	<0.29
RT Sco	232	0.035	-45.9	13.9	3.2	0.49	0.007:	-44:	28:	3.1	0.21
W Aql	24	0.148	-25.1	24.2	10.3	3.7	0.150	-23.2	22.0	10.5	4.5
DK Vul	196	0.009:	-22.0:	14.0:	4.6	0.11	—	—	—	4.1	<0.27
RZ Sgr	228	0.029	-29.7	8.5	3.0	0.27	—	—	—	2.9	<0.21
π^1 Gru	288	0.014	-10.5	20.2	1.7	0.28	—	—	—	2.3	<0.20
IRC+10°216	4	2.41	-25.4	22.1	22.8	53.8	8.33	-22.5	17.2	23.7	199.

[a] Gaussian fit parameters

[b] parabolic fit parameters

3.1. Statistical equilibrium model

We used the statistical equilibrium code described in Bieging & Tafalla (1993) to determine the populations of molecules in rotational levels in both the ground and first vibrationally excited states. Briefly, the statistical equilibrium equations are solved iteratively, including both collisional and radiative excitation, for an expanding spherical envelope. Radiative transfer for the exciting photons is treated by an escape probability formalism (Castor 1970). This approach is appropriate for these stars, since the expansion velocity is large compared to the local line width, so the large velocity gradient approximation is valid. The emergent spectrum is calculated by numerical integration of the transfer equation for a series of annuli in the projection of the envelope on the plane of the sky, and then convolved with the telescope beam.

The envelope density is determined by the gas mass loss rate, $\dot{M}_g$, and the expansion velocity, $V_{\rm e}$, both assumed constant with time. We further assume that the hydrogen is entirely molecular for calculating the collision rates. The outer extent of the envelope is not truncated; however, the drop in density and temperature (and for some models, molecular abundance) with radius effectively cuts off the molecular emission at some radius, beyond which the calculation is terminated.

The stellar radiation field is modelled as a 2000 K blackbody with a total luminosity of 1×10^4 L$_\odot$. The local (thermal and turbulent) velocity dispersion is assumed to be 1 km s^{-1}. The kinetic temperature of the envelope is assumed to depend on radius in an analytic form which approximates the results of Kastner (1992), who solved the equation of thermal balance for model CSEs as a function of mass loss rate. We adopt a kinetic temperature law of the form $T_K(r) = T_{\rm o}$ for $r < r_{\rm o}$, and $T_K(r) = T_{\rm o}(r/r_{\rm o})^{-0.7}$ for $r \geq r_{\rm o}$, where r is the distance from the star, and $T_{\rm o}$ and $r_{\rm o}$ depend on the mass loss rate. The exponent, -0.7, seems to be a good approximation to the radial dependence of T_K found by Kastner (1992), for mass loss rates covering the range applicable to our program stars.

Kastner (1992) notes that a significant uncertainty in the adopted temperature law is the nature of the circumstellar dust. The heating rate for gas-grain collisions depends on the grain emissivity and on the dust/gas ratio. Kastner (1992) used values appropriate for carbon stars. If S stars have mainly silicate grains (as indicated by their IRAS LRS spectra–see Sect. 4.2 below), his models based on graphite grains may overestimate the heating rates. If S stars also have a lower dust/gas ratio than carbon stars, on average, then the heating rate would also be too high. Both effects would tend to cause the adopted kinetic temperature law to be too large, by an uncertain factor. (On the other hand, a reduced dust/gas ratio might enhance the radiative heating of the dust, due to a reduction in the envelope opacity to stellar radiation.) The effect on the calculated SiO line intensities is likely to be small for most stars in our sample, however, since radiative excitation through the IR ro–vibrational lines dominates over collisional excitation for all except W Aql, with its relatively high mass loss rate.

3.2. SiO models

The IR ro-vibrational transitions for SiO were calculated using molecular constants from Tipping & Chackerian (1981). Radiative transition rates were calculated from their values for the dipole moments for vibrational and pure rotational transitions. Collisional rates for the ground vibrational state of SiO were derived from the rate coefficients described in Turner et al. (1992). We used an approximation to the temperature dependence of the rate coefficients of the form

$$\gamma_{j,j'} = A(\Delta j)\, y \exp[-B(\Delta j) y^{1/4}] \times \exp[-C(\Delta j) y^{1/2}] \quad (1)$$

where $y = \Delta E/kT$ and the three parameters A, B, and C are functions of the difference in initial and final rotational quantum numbers, Δj. A, B, and C were determined by least squares fits to the Turner et al. (1992) rates (which were calculated for a range of temperatures from 20 to 1800 K). Eq. (1) is a modified version of the analytic approximation given by de Jong et al. (1975), and is motivated by the discussion in Albrecht (1983),

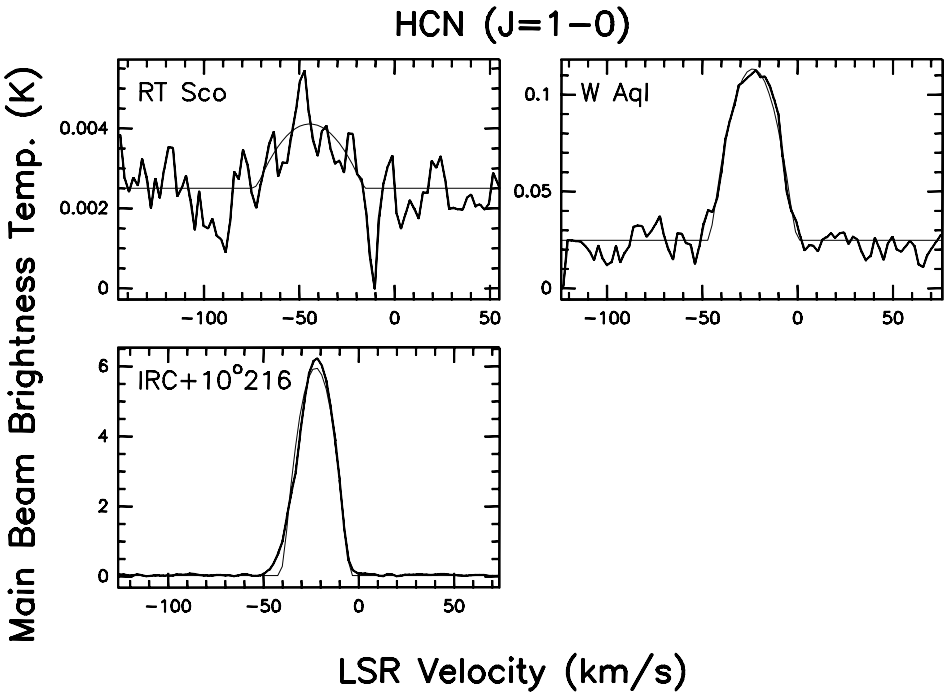

Fig. 2. Spectra of HCN J=1-0 detections. Thin line shows parabolic least-squares fit, with parameters given in Table 2.

but with an added term in the exponent to improve the fit over a wider range in T_K. For kinetic temperatures above 100 K, Eq. (1) gives rates which differ from the quantum mechanical calculations by less than 50%, and are generally better than that at higher T_K. We neglect collisional excitation to the vibrationally excited levels, for which the rates are small compared to the corresponding radiative rates in these models.

Given the uncertainty in the distribution of SiO, we have tried to constrain the range of abundances by considering two types of models. In the simplest case, we take the SiO abundance to be constant throughout the envelope. In reality, SiO molecules are presumably formed in the photosphere but removed from the gas by grain formation and photodissociation. We therefore expect the true SiO distribution to have a maximum abundance close to the star and to fall off with increasing distance. Since our data consist of only beam-averaged spectra, the constant abundance model should constrain the photospheric SiO value as a firm lower limit.

The predicted SiO J=3-2 spectrum (convolved with the SEST beam) for W Aql and a constant abundance model is compared with the observed spectrum in Fig. 3.

A second, more realistic model for the distribution is an exponential fall-off in SiO abundance with increasing distance from the star. We have calculated exponential models of the form $X_{\rm SiO} = X_c \exp(-r/r_e)$ where $X_{\rm SiO}$ is the abundance of SiO with respect to H_2 (assumed to be the only significant form of hydrogen), X_c is the central or photospheric abundance, and r_e is the e-folding distance. This distribution is a reasonable approximation to the form of the distribution derived for 3 stars, including the S star χ Cyg, by Sahai & Bieging (1993) based on interferometer images of the SiO J=2-1 emission. We further restrict the exponential model by fixing the e-folding distance,

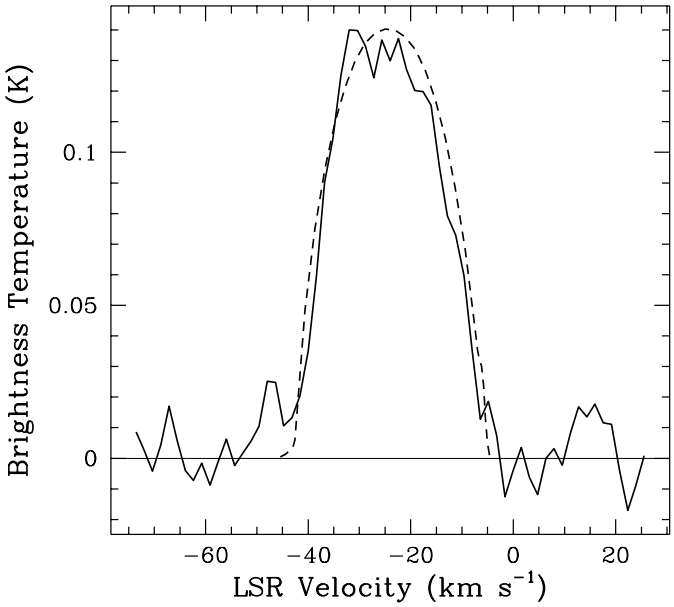

Fig. 3. Sample of SiO (v=0, J=3-2) model spectrum *(dashed line)* compared with observed spectrum *(solid line)* for W Aql

r_e, at 3×10^{15} cm, a value which produces satisfactory agreement with the observed SiO J=2-1 brightness distribution for χ Cyg (Lucas et al. 1992; Sahai & Bieging 1993).

The parameters of the excitation models, and the abundances which reproduce the observed beam-smoothed brightness temperatures in the model spectra, are summarized in Table 3. Columns 2 and 3 give the parameters of the adopted kinetic temperature law for each star, which depend on the mass loss rate. This rate is given in column 4, and is taken from the CO results of BL, Sahai & Liechti (1995), or Sahai (1992) (for π^1

Table 3. Excitation model parameters and derived abundances for SiO and HCN

Star	Kinetic temp. law				SiO models		HCN model	
					constant	exponential		
	r_o (cm)	T_o (K)	$\dot{M}_g$ ($M_\odot$ yr^{-1})	V_e (km/s)	X_o	X_c	r_{ph}	X_c
(a) S stars detected at SEST *(this paper)*								
R Gem	5E15	2000	2.4E-7	5.4	3.E-6	4.E-5	—	—
ST Sco	5E15	2000	9.0E-8	7.1	1.7E-6	1.4E-5	—	—
RT Sco	3E15	2000	6.1E-7	11.0	1.0E-6	1.0E-5	3E15	6E-6
W Aql	2E15	600	6.5E-6	18.7	2.2E-6	$\geq$4E-5	1E16	$>$5E-6
DK Vul	5E15	2000	2.8E-7	5.0	4.E-7	4.E-6	—	—
RZ Sgr	3E15	2000	6.4E-7	8.8	1.2E-6	$\geq$1.7E-5	—	—
π^1 Gru	3E15	2000	5.0E-7	11.0	5.E-8	3.0E-7	—	—
(b) Additional S stars detected by Bieging and Latter (1994)								
R And	3E15	2000	5.5E-7	9.3	1.0E-6	2.7E-5	3E15	2E-5
S Cas	2E15	600	4.6E-6	22.0	5E-6	8E-5	8E15	$>$4E-5
W And	5E15	2000	2.7E-7	7.8	4.5E-6	5E-5	—	—
χ Cyg	5E15	2000	2.6E-7	9.5	1.8E-6	3.2E-5	2E15	$>$4E-6

Gru). The value of the envelope expansion velocity, given in column 5, is from Table 1 for the SEST sample, or from BL for the 4 additional stars in Table 3(b). Column 6 gives the value, X_o, for a constant SiO abundance model which should be a lower limit to the photospheric value. Column 7 gives the corresponding central abundance, X_c, for an exponential model with an e-folding distance of 3×10^{15} cm.

Besides the stars observed at SEST in the SiO v=0, J=3-2 line, we have also calculated SiO abundance models for the 4 northern S stars detected in the v=0, J=2-1 line with the NRAO 12-m telescope by BL. Values for these stars are listed in the second part of Table 3. The adopted values of mass loss rate and envelope expansion velocity for R And, S Cas, and W And are taken from BL. For χ Cyg we adopt the mass loss rate and expansion velocity from Jorissen & Knapp (1998), which are derived from observations of several CO transitions and assume the *Hipparcos* distance of 106 pc.

The range of values for the constant abundance models is relatively small for 10 of the 11 stars, with values between 0.4×10^{-6} and 5×10^{-6}. The star π^1 Gru is an exception, with a value of $X_o = 5 \times 10^{-8}$. The exponential models yield central (i.e., photospheric) abundances, X_c, between 4×10^{-6} and 8×10^{-5}, except for π^1 Gru, which has $X_c = 3 \times 10^{-7}$, more than an order of magnitude lower than for the other 10 stars. We note that in the case of χ Cyg, our exponential model yields a central SiO abundance $X_c = 3.2 \times 10^{-5}$, which is similar to that derived by Bujarrabal et al. (1989) for a comparable model calculation, though the functional forms of the SiO abundance differ. In their model, the limiting value of the SiO abundance at large radii is 1.5×10^{-6}, close to our best-fit constant abundance model at $X_o = 1.8 \times 10^{-6}$.

The exponential models for SiO produce (v=0, J=3-2) line opacities which are only moderately optically thick. For example, the best-fit exponential model for RT Sco reaches a peak tangential optical depth of 0.9 at a radius of 6×10^{15} cm. RT Sco has a moderate mass loss rate, typical of most stars in our sample. In the case of very high mass loss rates, such as W Aql, the SiO model opacities may be large enough that the derived SiO abundance should be considered lower a limit, as indicated in Table 3. For most of the stars in our sample, however, the SiO lines are not very optically thick and our derived abundances should be reliable (within the context of the assumed model abundance distribution).

3.3. HCN models

Models for HCN emission followed the analysis applied to the carbon star IRC+10°216 by Dayal & Bieging (1995). The same statistical equilibrium code was used as for the SiO analysis described in the previous section. Collision cross sections for HCN were derived from Green & Thaddeus (1974), and molecular constants were from Maki (1974) and Evans et al. (1991). The stellar properties are the same as those used in the SiO models, including mass loss rates, wind velocities, and kinetic temperature law.

The abundance distribution of HCN is unknown since the formation mechanism is uncertain for S stars. In this analysis, we assume that HCN is formed close to the star (rather than in an extended photochemical region) and is carried out in the stellar wind. At sufficiently large radii, the HCN is photodissociated by ambient UV photons penetrating the dusty circumstellar envelope. With this assumption, the HCN abundance distribution should be similar to that of carbon stars such as IRC+10216. Following Olofsson et al. (1998) we parametrize the photodissociation radius for HCN as a function of the gas mass loss rate,

$\dot{M}_g$ (in solar masses per year), and wind velocity, $V_{\rm exp}$ (in km/s), as

$$r_{ph} = \left(\frac{V_{\rm exp}}{G_o}\right) + 2.9\times10^{15}\left(\frac{\dot{M}_g}{10^{-6}}\right)^{0.7}\left(\frac{V_{\rm exp}}{10}\right)^{-0.4}\ {\rm cm} \quad (2)$$

where $G_o = 1.1\times10^{-9}$ s^{-1} is the unshielded photodissociation rate of HCN (van Dishoeck 1988). The second term in this formula assumes that the dust in the circumstellar envelope provides shielding typical for carbon stars. Given this assumption, the HCN photodissociation radii for the detected stars are given in column 8 of Table 3, calculated from Eq. (2) and the values in columns 4 and 5.

The model abundance distribution is taken to be a gaussian centered at the star with an e-folding radius r_{ph} as given by Eq. (2), i.e., $X_{HCN}(r) = X_c{\rm exp}(-r/r_{ph})^2$. The model central or "photospheric" abundance of HCN is then given by X_c. Statistical equilibrium models were calculated, varying X_c to obtain a predicted line intensity (convolved to the SEST telescope beam) which is equal to the observed value (see Table 2). We have also calculated HCN abundance models for the northern S stars detected in the HCN J=1-0 line by BL. The model spectra for these stars were convolved to the 72" HPBW of the NRAO 12-m telescope. Results for stars in both samples are given in the last two columns of Table 3.

For RT Sco, the signal to noise ratio of the HCN spectrum is not high, so the model fit is uncertain by of order a factor of 2. For W Aql, the HCN line is strong and has good signal to noise ratio, but is clearly parabolic in shape, indicating optically thick emission. The fitted HCN abundance must therefore be considered a lower limit. The same comment applies to S Cas and χ Cyg, detected by BL.

It should be emphasized that these models assume a near-photospheric origin for HCN, with destruction by photodissociation at a characteristic radius given by Eq. (2). If HCN in these stars were produced by photochemical processes in the outer envelope (e.g., involving dissociation of N_2 and CH_4–cf. Willacy & Millar 1997; Charnley et al. 1995), then the foregoing analysis would be inappropriate. Without a resolved image of the HCN emission, however, there are too many free parameters to make alternative (i.e., photochemically-produced) HCN abundance models of much use at present.

4. Discussion

4.1. SiO abundances

The SiO abundances inferred from our models for the observed SiO (v=0, J=2-1 and J=3-2) line intensities seem to be consistent with those expected for stars with C/O = 0.95 - 1.00, which is the range expected for S stars. Sharp & Wasserburg (1995) have considered the composition of the gas and dust condensates in AGB star atmospheres in this range, and note that SiO should take up essentially all O not in CO, with SiO falling to near zero abundance only at C/O = 1.00. We assume that our program stars have silicon abundances equal to the solar value, Si/H_{tot} = 3.6×10^{-5} (Anders & Grevesse 1989). Then, if Si is fully associated with O as SiO, and all H is in H_2, the maximum SiO abundance, X(SiO), is 7.1×10^{-5}. For comparison, our lower limits on X(SiO) for the constant abundance models (column 6 of Table 3) are in the range (0.4 - 5)$\times10^{-6}$, except for π^1 Gru with X_o (SiO) = 5×10^{-8}, i.e., well below the upper limit set by the abundance of Si. The presumably more realistic models, with an exponential decline in X(SiO) with increasing distance from the star, yield central abundances an order of magnitude larger, X_c = (0.4 - 8)$\times10^{-5}$ (again, except for π^1 Gru at 3×10^{-7}). These values would imply that between 5% and ∼100% of Si is in gas-phase SiO in the inner envelope, in the zone where dust condensation occurs.

This range of SiO abundances for the exponential model is consistent with values expected if SiO is formed under conditions of thermodynamic equilibrium, for reasonable stellar parameters. For example, the TE chemical models calculated by Latter (in BL) predict that X(SiO) is on the order of a few $\times10^{-5}$ for C/O $\leq$ 0.97, T $\leq$ 2300 K, and $n_{tot} \approx 10^{12}$ cm^{-3}. The C/O ratio inferred for the S stars classified by Ake (1979) and by Keenan & Boeshaar (1980) with abundance indices like those of our program stars, are in this range, C/O = 0.95 - 0.97. The temperature classes range from S4 to S8 (see Table 1), which according to Ake (1979) correspond to color temperatures in the range 3200 - 1800 K. The photospheric temperature is not, of course, representative of the gas temperature in the extended atmosphere in which the SiO is assumed to form, which is likely to be cooler than the photosphere. The spectral classifications at least imply temperatures sufficiently low to permit formation of SiO at large abundances (i.e., approaching the limit set by the Si abundance and the available free O).

The model SiO abundances also suggest that if TE chemistry is the formation mechanism, then the total density in the relevant part of the stellar atmosphere must be in the vicinity of $\sim 10^{12}$ cm^{-3} and cannot be much lower (e.g., 10^{10} cm^{-3}). The inferred SiO abundances could then be used to constrain atmospheric models for these stars.

An important caveat in considering the TE chemical models for forming SiO, however, is whether TE is even relevant. All of the program stars are variables, and like other red giants, presumably have pulsation-driven shocks periodically passing through their extended atmospheres. If so, the effects of shocks on the atmospheric chemistry may be substantial. As an example, Willacy & Cherchneff (1998) have calculated molecular abundances in gas undergoing periodic shocks in a carbon-rich stellar atmosphere (specifically, for IRC+10°216). They find that, in the carbon-rich case (C/O = 1.5), the SiO abundance is strongly enhanced over the TE value, by one or two orders of magnitude depending on the shock velocity. Thus, in the case of carbon stars the SiO abundance is probably determined by shock processes, not TE chemistry near the photosphere.

It is not clear whether this conclusion would apply to S (or M) stars, however. In carbon stars, Si is mainly in atomic Si and in SiS, with SiO a very minor carrier of Si. In S (and M) stars, SiO is predicted to be a major form of gas-phase silicon. Detailed calculations of the chemical effects of shocks in M and S stars would be of great interest.

The anomalously low SiO abundance derived for π^1 Gru is noteworthy. Sahai (1992) discovered that the CO emission for the circumstellar envelope of this star was bipolar in morphology and that the CO J=2-1 and 1-0 lines showed relatively broad wings. He argued that these wings and the CO morphology implied that a fast bipolar outflow was being collimated by a dense torus of gas within the slower, presumably older outflow. If the interaction of these velocity components produces shocks, our analysis would suggest that SiO abundance is lowered as a result. The location of such shocks would presumably be in the extended circumstellar envelope, however, not in the stellar atmosphere. Alternatively, if the bipolar envelope is an indication that π^1 Gru is already evolving off the AGB, there may simply be little circumstellar molecular gas in the vicinity of the star, due to a cessation of mass loss.

4.2. Composition of the dust

The type of dust formed is obviously related to the composition of the gas in AGB star atmospheres, as well as to the temperature and pressure. With the special chemical properties of S stars, especially C/O near 1, the character of the circumstellar dust is of interest for comparison with the molecular composition of the gas. Sharp & Wasserburg (1995) predicted that with 0.95 $<$ (C/O) $<$ 1.00, silicates and oxides should condense, but not graphite or silicon carbide grains. (They note, however, that the sensitivity of their calculations to the somewhat uncertain thermodynamic data for grain condensation makes quantitative prediction difficult in this range of C/O.)

One set of observational data on the nature of circumstellar dust are the IRAS LRS spectra. Chen & Kwok (1993) made a detailed examination of the spectra for all known S stars in the LRS database, including the stars in our sample. Four stars (ST Sco, RT Sco, W Aql, and π^1 Gru) have class E spectra, i.e., showing the 9.7 micron silicate feature in emission. Three stars (R Gem, DK Vul, and RZ Sgr) are in class F, indicating a featureless dust continuum. (We note that the LRS spectra are not of uniformly good quality. The S/N ratio of the spectrum of DK Vul is rather low and may admit a weak 9.7 micron emission feature masked by noise.) None of these stars is classified as having an 11.3 micron silicon carbide feature (class C) or a stellar continuum (class S). The preponderance of class E LRS spectra is qualitatively consistent with our 100% detection rate of SiO and the relatively large inferred abundances of SiO, and with the absence of SiC emission features at 11.3 microns. The case of the featureless dust continuum (class F) is less clear. RX Sgr has an apparently featureless continuum with good S/N in the LRS spectrum, yet it also displays a well-detected SiO line and a relatively high inferred SiO abundance. Evidently the presence of SiO in the gas phase is no guarantee that the 9.7 micron silicate feature will be seen. The 3 stars in our present sample which Chen & Kwok (1993) classify as having F type LRS spectra are among the higher photospheric temperature classes (S4 or S5) in our sample. Higher gas temperature may favor the formation of oxide grains (e.g., Al_2O_3) rather than silicates, so that the 9.7 micron feature is suppressed because of a difference in grain composition (see Sharp & Wasserburg 1995; Sedlmayr & Krueger 1997).

4.3. Formation of HCN

Finally, we consider the problem of the detection of HCN in some S stars. In our present sample, we find a weak detection of HCN J=1-0 in RT Sco, and a strong detection in W Aql. The latter star was also detected by BL, as well as 3 others (R And, S Cas, and χ Cyg). Thus, 5 S stars out of 15 surveyed for HCN emission are detected in the J=1-0 line.

The HCN abundance is uncertain because the molecular distribution is unknown. If we assume that HCN is formed close to the star, and is photodissociated at a radius given by (2), we infer initial abundances of at least a few $\times 10^{-6}$ with respect to H_2. Such large HCN abundances cannot easily be explained by gas phase TE chemistry. From the models of Latter (cf. BL), there is perhaps only a small corner of parameter space that could accommodate the inferred abundances of both SiO and HCN in this picture, i.e., if C/O $\geq$ 0.97, T $<$ 1300 K, and $n_{tot} \approx 10^{12}$ cm^{-3}. The inferred SiO abundance is a fairly strong constraint that C/O $\leq$ 0.97, which is also consistent with the spectroscopic abundance indices (Ake 1979, Keenan & Boeshaar 1980). It could be that Eq. (2) underestimates the HCN photodissociation radius, r_{ph}. If so, our values for the HCN abundances in Table 3 would be too large. Eq. (2) was derived for carbon stars, but S stars may have lower dust/gas ratios than is typical of carbon stars (cf BL; Sahai & Liechti 1995). Thus it seems at least as likely that Eq. (2) overestimates r_{ph} as underestimates it. Interferometric images of the HCN emission would be very helpful to settle this question.

At such low gas temperatures, however, grain condensation is likely to be an important process, and could enhance HCN formation in the gas. Sharp (1988) argued that removal of O by condensation of silicate and/or oxide grains effectively raises the gas C/O and hence promotes the formation of HCN. This mechanism should be most effective for S stars with C/O $\approx$ 0.95 - 0.97. The star χ Cyg may be problematic, since it has strong HCN emission (cf. BL) but a relatively low C/O index, probably with C/O $\approx$ 0.9 (Keenan & Boeshaar 1980).

A second possibility, also invoked to explain the presence of HCN in M-type stars is that HCN is formed by photochemical reactions in the outer envelope (Nercessian et al. 1989; Charnley et al. 1995; Willacy & Millar 1997). It is not clear that this mechanism is consistent with the expected abundances of likely precursor molecules, i.e., CH_n, n = 2,3,4. Even in the C-rich model of Willacy & Cherchneff (1998), the TE abundances of CH_n species are low and are not enhanced by shocks (except CH_4 in relatively strong shocks). One would expect that CH_n abundances are correspondingly much lower in the case of C/O $\leq$ 0.97, typical of S stars, than in the case C/O = 1.5. Thus, a photochemical origin for HCN leads to the problem of the formation of the precursor simple hydrocarbons, CH_n.

One may also speculate about the effects of shocks in generating HCN directly in S stars. The calculations of Willacy & Cherchneff (1998) find that in the carbon-rich case (C/O = 1.5),

shocks destroy HCN, and lower the abundance by about a factor of 6 compared to the TE values. In the absence of detailed calculations for C/O ≈ 1, it is difficult to predict whether HCN might be enhanced by shocks, but this mechanism does not appear promising as an explanation for the presence of detectable HCN in $\sim$30% of S stars surveyed.

5. Summary and conclusions

We have presented the results of a search for SiO (v=0, J=3-2) and HCN J=1-0 line emission from a sample of southern S stars, using the SEST telescope. The seven stars observed all show evidence of circumstellar envelopes created by mass loss, as indicated by relatively strong CO lines and excess emission in the IRAS bands. We use a statistical equilibrium/radiative transfer code for spherical shells to determine, or at least constrain, the molecular abundances of SiO and HCN for the stars detected in this survey as well as those detected by BL. The observations and analysis lead to the following conclusions.

(1) The SiO (v=0, J=3-2) line is detected in all 7 stars. Excitation models which assume a constant SiO abundance, X(SiO), provide a lower limit to X(SiO) in the range (0.4-5) $\times\ 10^{-6}$. A more realistic model, where the SiO abundance falls off exponentially with distance from the star, with an e-folding radius of 3×10^{15} cm, gives photospheric SiO abundances in the range (0.4-8) $\times\ 10^{-5}$. The star π^1 Gru is an exception, with an order of magnitude lower SiO abundance than the other stars in our sample.

(2) The detection and inferred abundances of SiO are consistent with formation of the molecule under TE conditions near the stellar photosphere, if C/O $\sim$ 0.97 is typical of these S stars, and the gas density and temperature are $n\ \sim\ 10^{12}$ cm^{-3} and T $\leq$ 2300 K, according to the chemical models presented in BL. However, the formation of SiO may be controlled by the passage of pulsationally-driven shocks through the stellar atmosphere, if the models of Willacy & Cherchneff (1998) for carbon star atmospheres are also applicable to S stars.

(3) The HCN J=1-0 line is detected in 2 of the 7 southern S stars observed. This detection rate is comparable to that by BL for northern S stars. All S stars in the present work and in BL, which are detected in HCN emission, show the 9.7 micron silicate feature in emission in IRAS LRS spectra (Chen & Kwok 1993).

(4) If HCN is produced near the stellar photosphere, our models require abundances which are much higher than predicted by TE chemistry, unless the gas temperature is $<$1300 K and the density n(H_2) $\sim 10^{12}$ cm^{-3}. Such conditions would also be likely to result in grain formation. HCN production could then be enhanced if condensation of silicate (or oxide) grains resulted in an increase in the gas-phase C/O ratio to be ≈ 1, as proposed by Sharp (1988). Such a scenario would be consistent with the presence of the 9.7 micron silicate feature in emission in these stars. Alternatively, HCN formation may occur through photochemical reactions in the outer envelope. If so, a measurement of the size of the HCN distribution is necessary to estimate the HCN abundance. Interferometric imaging of HCN emission in these stars is needed to discriminate between the possible chemical origins.

Acknowledgements. WBL thanks the U.S. National Radio Astronomy Observatory for support during the initial phases of this work. JHB acknowledges support from the U.S. National Science Foundation through grant AST 96-18523. HO acknowledges financial support from the Swedish Natural Science Research Council. We thank Ms. Shanna Shaked for assistance with the figures.

References

Ake T.B. 1979, ApJ 234, 538
Albrecht M.A. 1983, A&A 127, 409
Anders E., Grevesse N. 1989, Geochim. Cosmochim. Acta 53, 197
Bieging J.H., Latter W.B. 1994, ApJ 422, 765 (BL)
Bieging J.H., Tafalla M. 1993, AJ 105, 576
Booth R.S., Delgado G., Hagström M., Johansson L.E.B., Murphy D.C. 1989, A&A 216, 315
Bujarrabal V., Gomez-Gonzalez J., Planesas P. 1989, A&A 219, 256
Bujarrabal V., Fuente A., Omont A. 1994, A&A 288, 551
Castor J.I. 1970, MNRAS 149, 111
Chan S.J., Kwok S. 1991, ApJ 383, 837
Charnley S.B., Tielens A.G.G.M., Kress M.E. 1995, MNRAS 274, L53
Chen P.S., Kwok S. 1993, ApJ 416, 769
Danchi W., Bester M. 1995, Ap&SS 224, 339
Dayal A., Bieging J.H. 1995, ApJ 439, 996
deJong T. 1989, A&A 223, L23
deJong T., Chu S.-I., Dalgarno A. 1975, ApJ 199, 69
Evans N.J. II, Lacy J.H., Carr J.S. 1991, ApJ 383, 674
Gezari D.Y., Schmitz M., Pitts P.S., Mead J.M. 1993, NASA Ref. Publ. 1294
Green S., Thaddeus P. 1974, ApJ 191, 653
Groenewegen M.A.T., de Jong T. 1998, A&A 337, 797
Jorissen A., Knapp G.R. 1998, A&AS 129, 363
Jorissen A., Mayor M. 1992, A&A 260, 115
Jorissen A., Frayer D.T., Johnson H.R., Mayor M., Smith V.V. 1993, A&A 271, 463
Jura M. 1988, ApJS 66, 33
Kastner J. 1992, ApJ 401, 337
Keenan P.C., Boeshaar P.C. 1980, ApJS 43, 379
Kutner M.L., Ulich B.L. 1981, ApJ 250, 341
Kutner M.L., Mundy L., Howard R.J. 1984, ApJ 283, 890
Little S.J., Little-Marenin I.R., Hagen-Bauer W. 1987, AJ 94, 981
Lucas R., Bujarrabal V., Guilloteau S. et al. 1992, A&A 262, 491
Maki A.G. 1974, J. Phys. Chem. Ref. Data 3, 221
Nercessian E., Guilloteau S., Omont A., Benayoun J.J. 1989, A&A 210, 225
Neugebauer G., Leighton R.B. 1969, Two Micron Sky Survey (NASA SP-3047)(TMSS)
Olofsson H., Eriksson K., Gustafsson B., Carlström U. 1993, ApJS 87, 305
Olofsson H., Lindqvist M., Nyman L-Å., Winnberg A. 1998, A&A 329, 1059
Sahai R. 1992, A&A 253, L33
Sahai R., Bieging J.H. 1993, AJ 105, 595
Sahai R., Liechti S. 1995, A&A 293, 198
Schieder R., Tolls V. Winnewisser G. 1989, Exp. Astron. 1, 101
Sedlmayr E., Krueger C. 1997, in Astrophysical Implications of the Laboratory Study of Presolar Materials, eds. T. Bernatowicz and E. Zinner, AIP Press, p. 425

Sharp C.M. 1988, in Rate Coefficients in Astrochemistry, eds. T. Millar and D. Williams (Dordrecht: Kluwer), p. 309
Sharp C.M., Wasserburg G.J. 1995, Geochim. Cosmochim. Acta 59, 1633
Stephenson C.B. 1984, Pub. Warner and Swasey Obs., Vol. 3, No. 1 (S2)
Tipping R.H., Chackerian C. 1981, JMolSpec 88, 352
Turner B.E., Chan K.-W., Green S., Lubowich D.A. 1992, ApJ 399, 114
van Dishoeck E.F. 1988, in Rate Coefficients in Astrochemistry, eds. T.J. Millar and D.A. Williams, Kluwer, Dordrecht, p. 49
Van Eck S., Jorissen A., Udry S., Mayor M., Pernier, B. 1998, A&A 329, 971
Willacy K., Cherchneff I. 1998, A&A 330, 676
Willacy K., Millar T.J. 1997, A&A 324, 237
Zuckerman B., Maddalena R.J. 1989, A&A 223, L20